ELSEVIER

Earth and Planetary Science Letters 192 (2001) 457–470

EPSL

www.elsevier.com/locate/epsl

Incompatible element-rich fluids released by antigorite breakdown in deeply subducted mantle

Marco Scambelluri [a,*], Piero Bottazzi [b], Volkmar Trommsdorff [c], Riccardo Vannucci [b,d], Joerg Hermann [e], Maria T. Gòmez-Pugnaire [f], Vicente Lòpez-Sànchez Vizcaìno [g]

[a] *Dipartimento per lo Studio del Territorio e delle sue Risorse, Università di Genova, Corso Europa 26, 16132 Genova, Italy*
[b] *C.S. Cristallochimica Cristallografia, CNR, Pavia, Italy*
[c] *Institut fur Mineralogie und Petrographie, ETH Zentrum, Zurich, Switzerland*
[d] *Dipartimento di Scienze della Terra, Università di Pavia, Pavia, Italy*
[e] *Research School of Earth Sciences, Australian National University, Canberra, ACT 0200, Australia*
[f] *Departamento de Mineralogia y Petrologia, Universitad de Granada, Granada, Spain*
[g] *Departamento de Geologia, Universidad de Jaén, Jaén, Spain*

Received 28 February 2001; received in revised form 19 July 2001; accepted 19 July 2001

Abstract

We present first trace element analyses of the fluid produced during breakdown of antigorite serpentine, a major dehydration reaction occurring at depth within subducting oceanic plates. Microinclusions filled with crystals+aqueous liquid are disseminated within olivine and orthopyroxene grown at pressures and temperatures beyond the stability field of antigorite. Despite hydrogen loss and significant major element changes that have affected the analyzed inclusions, their trace element composition still reflects characteristics of the subduction fluid released during serpentinite dehydration. The fluid is enriched in incompatible elements indicating either (1) interaction with fluids derived from crustal slab components, or (2) dehydration of altered (serpentinized) oceanic mantle previously enriched in incompatible elements. Several features of the analyzed fluid+mineral inclusions (high Pb/Th, Pb/U and Pb/Ce) are in agreement with available experimental work, as well as with the geochemical signatures of most arc lavas and of several ocean island basalt mantle sources. The trace element patterns of the fluid+mineral inclusions do not display relative enrichment in large ion lithophile elements compared to high field strength elements, thus suggesting that the latter elements may become soluble in natural subduction fluids.

Keywords: subduction; antigorite; fluid inclusions; trace elements

1. Introduction

Recent research on subduction zone metamorphism has concentrated on the nature and composition of fluids evolved during burial and heating of downgoing plates. Aqueous fluids are incorporated in the oceanic lithosphere during hy-

* Corresponding author. Tel.: +39-010-3538315; Fax: +39-010-352169.
E-mail address: msca@dipteris.unige.it (M. Scambelluri).

0012-821X/01/$ – see front matter
PII: S0012-821X(01)00457-5

drothermal circulation at ridge settings and flux the mantle above subduction zones, to create arc volcanism at convergent plate margins. Release of fluids from a descending slab is accompanied by cycling of crustal components into a hydrous fluid and/or a melt phase, the migration of which into the overlying mantle induces metasomatism and partial melting [1]. Uncertainties concern the nature and composition of fluid agents released during subduction because of the paucity of deep natural rocks and fluids available for analysis. Constraints on the nature of fluids liberated in the deep mantle by subduction are placed by several experimental investigations at high pressures and temperatures [2–5], and by studies of fluid inclusions in high to ultrahigh pressure rocks and in mantle xenoliths [6–9]. These indicate that mineral solubility in fluids increases with pressure, and that interactions between released fluid and host rocks can lead to formation of fluids loaded with dissolved rock components [10,11].

The trace element composition of fluids released at depth in subduction zones has been indirectly estimated by comparing primitive arc lavas with mid ocean ridge basalts (MORB), as well as by means of experimental studies of fluid–solid partitioning of trace elements at pressure–temperature conditions of the upper mantle [12–19]. These studies indicate that the agents fertilizing the mantle sources of arc magmas are characterized by an enrichment in large ion lithophile elements (LILE: Cs, Rb, Ba, Pb, U, Th, Sr) and light rare earth elements (LREE: La, Ce, Nd) with respect to high field strength elements (HFSE: Ti, Nb). Pb is more readily transported by such fluids than U and Th [17,19]: dehydration processes in the slab may thus produce large increases in U/Pb and Th/Pb of the residual subducting lithosphere, and may explain the low Ce/Pb ratios characteristic of arc magmas [20]. Since the fluids released during subduction experienced complex flow pathways into the mantle, it is yet unclear to what extent their LILE-enriched chemical signature is caused by dehydration of the slab, or by interaction of released fluids/melts with the mantle wedge [16,21,22]. However, direct trace element analyses of deep natural subduction fluids in high to ultrahigh pressure rocks are not available yet, and would be of considerable relevance to shed light on the above uncertainties. In this frame, subduction of hydrated, serpentinized oceanic mantle is an important variable [23], because breakdown of antigorite serpentine to olivine+orthopyroxene+water delivers 10–13 wt% bulk H_2O down to depths of 200 km. Antigorite breakdown therefore produces the largest amount of subduction fluids [24], the main features and compositions of which are yet unexplored. Here we report a textural and analytical study of primary fluid+mineral inclusions within olivine+orthopyroxene rocks from Cerro del Almirez (Betic Cordillera, SE Spain) which derive from subduction zone breakdown of antigorite serpentine. We show that these inclusions represent remnants of the metamorphic fluid phase evolved at antigorite breakdown, and we document that this fluid phase had high contents of incompatible elements.

2. Petrologic outline of olivine-orthopyroxene rocks at Cerro del Almirez

The high pressure transition from antigorite serpentinite to enstatite-olivine rock has been mapped at Cerro del Almirez [25], in ultramafic rocks closely associated with eclogites and metarodingites, and interlayered with metapelites, metaevaporites, marbles and graphite-bearing micaschists [26–28]. In the ultramafic rocks, subduction zone metamorphism overprints previous stages of oceanic hydration and alteration [25,26]. Ultramafites at Cerro del Almirez consist mainly of two rock types, serpentinites and spinifex-like olivine+enstatite rocks: these represent prograde stages of subduction zone recrystallization of hydrated oceanic mantle at increasing pressure and temperature. Serpentinites are made up of antigorite, olivine, diopside, tremolite and titanian clinohumite and represent an early stage of subduction crystallization in the presence of stable antigorite. At higher grades (pressure $>$ 1.5–2.2. GPa and 640–750°C) [25–27], antigorite breaks down to the assemblage enstatite+olivine+chlorite. This assemblage developed a spinifex-like texture, with radiating, cm-sized crys-

tals of enstatite and arborescent olivine indicating mineral growth in the presence of abundant fluid [25]. In the spinifex-like rocks, a first generation of olivine forms irregularly shaped clear cores, diffusely overgrown by rims of a second generation of olivine with brown pleochroism, due to the presence of numerous oriented submicroscopic particles of magnetite, chromite and ilmenite grown during crystallization of olivine [25–27].

3. Fluid inclusion petrography

The metamorphic olivines of both serpentinite and spinifex-like rocks contain fluid and fluid+mineral inclusions respectively. The metamorphic olivine ($X_{Mg} = 0.93$) and diopside of serpentinites locally contain primary to pseudosecondary two-phase (liquid+vapor) aqueous inclusions (Fig. 1A). These inclusions are confined to the antigorite serpentinites and are absent in the spinifex-like olivine: they are generally very small (5–10 μm) and occur either as isolated inclusions, or as core clusters inside olivine and diopside which coexist with antigorite in the metamorphic paragenesis that pre-dates the spinifex-like olivine and orthopyroxene. This inclusion assemblage may therefore represent a generation of aqueous subduction fluid produced prior to antigorite breakdown and growth of the spinifex-like olivine. In the latter olivine (white and brown; $X_{Mg} = 0.89$), inclusions containing a high volume percentage of mineral precipitates plus a rim of liquid (hereafter fluid+mineral inclusions) are common and occur either as core clusters of primary inclusions (Fig. 1B,C), or as pseudosecondary inclusions along microfractures. These inclusion trails are confined to the inner part of single olivine crystals and never cut across the grain boundaries. All these primary to pseudosecondary inclusion patterns are cut by

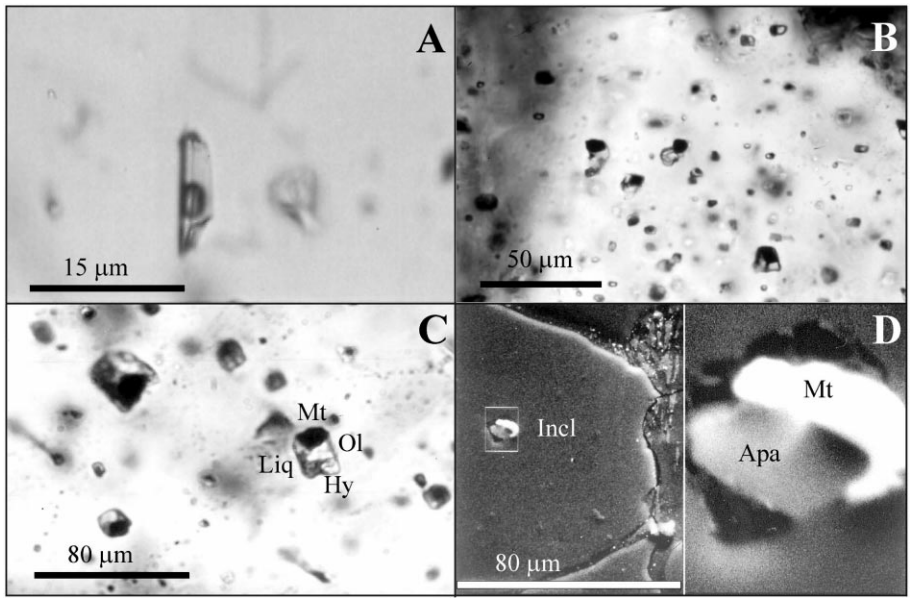

Fig. 1. Textural features of analyzed fluid inclusions. (A) Primary two-phase (liquid+vapor bubble) aqueous inclusion in metamorphic olivine from antigorite serpentinite samples. This olivine and the associated primary two-phase inclusions pre-date the crystallization of peak metamorphic spinifex-like olivine and formation of the associated fluid+mineral inclusions. (B, C) Close up view of primary fluid+mineral inclusions in the spinifex-like olivines. The inclusions display negative crystal shapes and constant volume ratios of infilling phases. These mainly consist of magnetite (black crystals in the inclusions), olivine (white grains in inclusions), a hydrous phase (white phase, similar to olivine) and a colorless liquid phase. Additional apatite can also be present. (D) Scanning electron microscope picture showing an opened magnetite+apatite inclusion in a spinifex-like olivine (left side of D). The inclusion has a regular shape, the black volume in the inclusion was likely occupied by a liquid phase. The right side of D shows in detail the apatite+magnetite infillings and the black inclusion edges.

late retrograde serpentine microfractures. The microfracturing indicates that fluid inclusion entrapment took place before late-stage infiltration of crustal fluids gave rise to formation of retrograde serpentine. The fluid+mineral inclusions prevalently display negative crystal shapes (Fig. 1B,C); under crossed polars the inclusion-filling silicates show regular shapes and birefringence, with extinction different from the one of the olivine host. In general, oxide, silicate and liquid phases inside the inclusions display constant volume proportions, consisting of approximately 30% oxide (magnetite), 50% silicate, 20% liquid (Fig. 1B,C). This constancy indicates that this inclusion generation trapped a homogeneous fluid, and recorded a common history of mineral precipitation from the fluid. Divergence from regular inclusion shapes and volume proportions of infilling phases is occasionally observed: in such cases the size of oxide crystals is highly variable, oxide locally appears as the dominant phase and the inclusion shape becomes irregular.

4. Analytical methods

Microthermometry of liquid+vapor inclusions in serpentinites was performed using a Linkam THMSG 600 heating–freezing stage calibrated on the melting point of pure CO_2 (−56.6°C) and H_2O (0.0°C), and on the critical point of pure water (371.4°C) in synthetic fluid inclusions. Error range is ±0.2°C for low-temperature measurements, and ±1.0°C at high temperature; heating rates were constantly kept at 0.1°C s^{-1}.

Scanning electron microscopy and analyses of solid phases in fluid+mineral inclusions in the spinifex-like olivine were made in energy dispersive mode by means of a Philips SEM 515 electron microscope at the University of Genova. The accelerating potential was 15 kV, the beam current 20 nA, the counting time 100 s. Natural mineral standards were employed.

Raman spectra of the mineral and liquid phases filling the inclusions inside spinifex-like olivine were obtained by means of a Dilor Labram II Microraman spectrometer with a He–Ne 632 nm laser equipped with a confocal microscope with a spectral resolution of 3 cm^{-1}. The instrument is available at the ETH Zentrum of Zurich.

Trace element analyses of solid phases in fluid+mineral inclusions were carried out by laser ablation microprobe–inductively coupled plasma–mass spectrometry (LAM–ICP–MS) at the CNR-CSCC in Pavia, Italy. The laser probe has a pulsed Nd:YAG laser source 'Brilliant' (Quantel, Les Ulis, France), with emission in the infrared (1064 nm) converted into 213 nm by means of three harmonic generators. The system was developed at the Memorial University of Newfoundland; its basic design and operation are described in Taylor et al. [29]. The particles produced by ablation were analyzed by a field-sector mass spectrometer ('Element', Finnigan MAT, Bremen, Germany), see [30] for details on RF power, gas flows into ICP torch and peak acquisition. For the present work, the laser operated at a repetition rate of 10 Hz, and with pulse energy of about 0.07 mJ. The ablation craters resulted slightly larger than the fluid+mineral inclusions, which averaged 30 μm size. Measured ion currents thus refer to fluid+mineral phases inside the inclusions, plus surrounding olivine hosts. Ion currents were integrated over the range defined by the steep rise and drop of signals of elements pertaining to inclusions and absent in olivine hosts, and were subtracted of the gas blank. Since olivine lacks all the trace elements measured in inclusions (Table 2), it does not contribute to the trace element ion currents and the derived relative concentrations pertain to the bulk inclusion only. Loss of material, from either the liquid or the solid phases, cannot be ruled out. However, it would be governed by the relative position of the phases within the inclusions, i.e. an aleatory phenomenon that should result in random effects. While this could account for part of the scatter observed, the consistency of the chondrite-normalized patterns for several inclusions indicates that the loss of material, if any, does not influence to a great degree the relative to Y ratios. Analyses of host olivine were carried out in inclusion-free areas according to the standard protocol given in [31] to determine its trace element concentration which resulted below detection limits. Owing to the lack of a suitable internal standard, required to

calculate the sensitivity normalized to the mass of the sample, the usual quantification protocol for mineral analysis [31] could not be applied for the bulk inclusion, so that absolute concentrations were not estimated. However, it has been possible to calculate the concentration of trace elements relative to one of them (Y has been selected), as they all pertain to the fluid inclusions only (Fig. 3). The NIST glass SRM612 was used as the external standard as it was proved suitable to the purpose using UV laser ablation (see [32] for a discussion on the possible calibration strategies for fluid inclusions). Owing to their ablation behavior, described by the so-called fractionation index [33] which is similar to that of the reference element Y, matrix-induced elemental fractionation is expected to be negligible for all the elements here investigated except for Pb and, to a minor extent, Rb, Cs. For Pb, we obtained concentrations higher by as much as ~35% on a basalt glass under operating conditions similar to those of this work and with the same external standard. However, since the normalized Pb values are at least two orders of magnitude higher than LREE, this uncertainty does not influence the conclusions of this work. Effects on the ICP due to the introduction of sampled material of different composition – in particular the fluid phase – are also expected to be small owing to the small sample uptake. The Y-normalized trace element concentrations thus obtained are correct on a relative basis, that is, the shape of trace element patterns in a normalized spiderdiagram.

5. Fluid inclusions analysis

5.1. Early aqueous inclusions

Microthermometry was performed on the aqueous liquid+vapor inclusions hosted in olivine and diopside from serpentinites (Table 1). Inclusions display initial melting temperatures between −23 and −43.4°C, indicating presence of NaCl, $MgCl_2$ and $CaCl_2$ as main chloride species. Final melting temperatures between −3.2 and −11.6°C indicate moderate fluid salinities of 5.2–15.57 wt% chloride concentrations, here expressed as NaCl equivalents [34]. Total fluid inclusion homogenization always occurred to the liquid phase at relatively high temperatures (Table 1). The corresponding fluid inclusion isochores plot below the pressure–temperature conditions estimated on the basis of mineral thermobarometry of the associated eclogites, as well as below the stability field of olivine+orthopyroxene in ultramafic systems [25,26]. This points to retrograde density readjustment of these fluid inclusions.

5.2. Fluid+mineral inclusions in the spinifex olivine

Identification of solid phases in the fluid+min-

Table 1
Microthermometry of early aqueous inclusions in serpentinites

Inclusion	T_{mi} (°C)	T_{mf} (°C)	T_{htot} (°C)	Salinity (wt% NaCl)	Density (g cm^{-3})
AL9537 inc 1.2	−23.0	−10.8	379.8	14.77	0.76
AL9537 inc 1.2b	−36.8	−11.6	368.4	15.57	0.79
AL9537 inc 3.3	−28.0	−10.2	448.7	14.16	0.64
AL9537 inc 3.2	−26.1	−8.2	447.3	11.94	0.60
AL9539 inc 1.1	−41.0	−11.2	397.4	15.18	0.74
AL9539 inc 1.1b	−38.0	−7.2	295.7	10.74	0.83
AL9539 inc 1.2	−43.4	−3.2	309.6	5.16	0.75
AL9539 inc 1.3	−23.7	−5.3	314.5	5.24	0.78
AL9539 inc 2.3	−40.0	−4.4	296.4	6.96	0.79
AL9539 inc 2.4	−38.4	−6.4	334.1	9.71	0.76
AL9539 inc 2.5	−40.5	−6.1	323.5	9.32	0.78
AL9539 inc 2.6	−30.5	−5.0	319.4	7.81	0.76
AL9539 inc 2.7	−22.0	−7.1	308.7	10.61	0.81

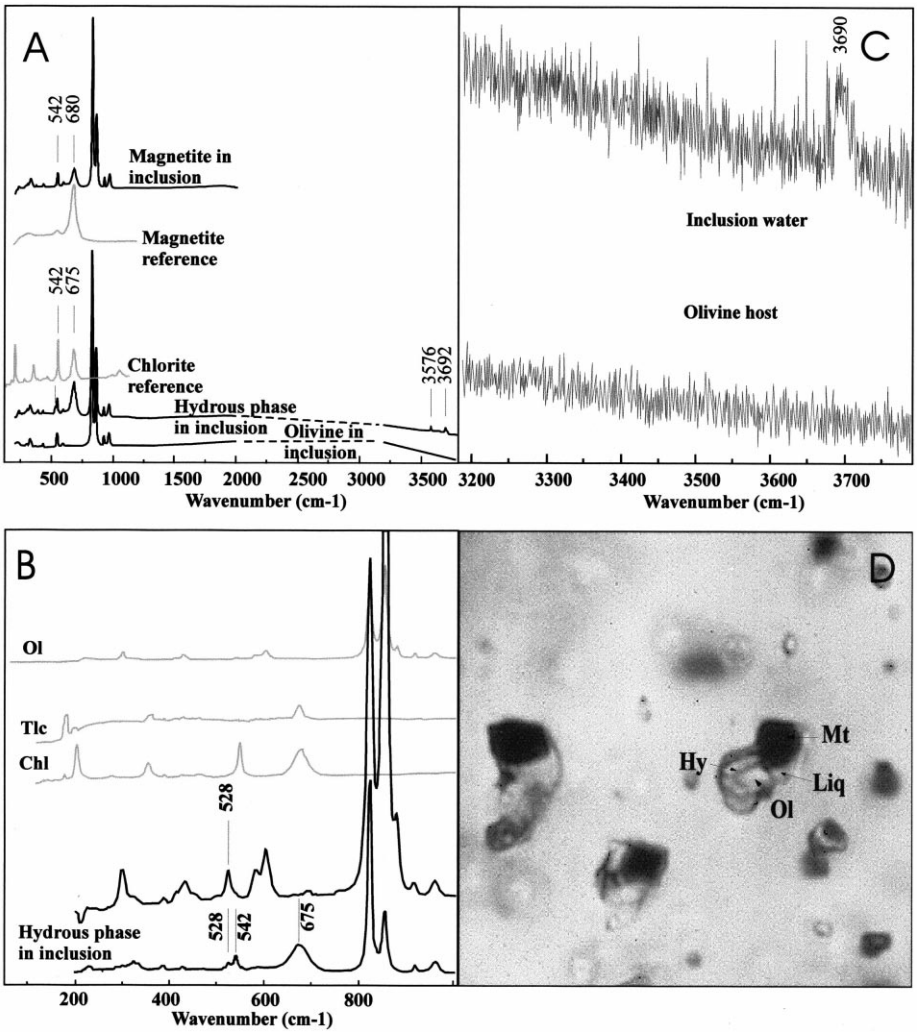

Fig. 2. Raman spectra of the various mineral phases in primary fluid+mineral inclusions in spinifex-like olivine. (A) Raman spectra of magnetite, olivine and hydrous phase (with peaks at 3576 and 3692 cm^{-1}) in the inclusions (black spectra). Reported for comparison are the reference spectra (in gray) of magnetite and chlorite. (B) Raman spectra of inclusion hydrous phase (in black) at wave numbers between 200 and 1000 cm^{-1}. Reported for comparison are the spectra of reference chlorite, talc and olivine (in gray). (C) Raman spectrum of the inclusion liquid phase showing a peak at 3690 cm^{-1}, typical of an aqueous fluid. Also reported is the spectrum of a spinifex-like olivine host. (D) Micrograph of the analyzed inclusions, showing infilling magnetite, olivine and hydrous phase together with a thin rim of liquid aqueous fluid at the inclusion walls.

eral inclusions was done in situ by means of direct Raman and scanning electron microscope analyses. The Raman microprobe analysis of minerals in these olivine-hosted inclusions was complicated by the interference of several peaks of the host olivine at wavelengths of 325, 428, 540, 824, 856, 919, 961 cm^{-1} (Fig. 2A). Despite this difficulty, olivine and magnetite (the latter with peaks at 542, 680 cm^{-1}) have been identified as mineral phases inside the inclusions (Fig. 2A, compare with Fig. 2D). Another common mineral in the inclusions shows peaks at 3576, 3692 cm^{-1}, i.e. at wave numbers typical of hydrous phases, and peaks at 542, 675 cm^{-1} (Fig. 2A,B), which compare well with the reference spectrum of chlorite (Fig. 2B). The Raman spectrum of the liquid in-

side the fluid+mineral inclusions has a peak at about 3690 cm^{-1}, which is characteristic of water (Fig. 2C). Scanning electron microscopy of opened inclusions inside the spinifex-like olivine indicates that inclusion cavities contain magnetite and olivine associated with a hydrous phase corresponding to chlorite; chlorine-bearing apatite (average dimensions <5 μm; Cl^- about 2.5 wt%) has also been found in the inclusions (Fig. 1D). The fluid+mineral inclusions thus contain a mineral assemblage of magnetite+olivine+chlorite+aqueous fluid ± Cl-apatite. Absence of antigorite among the mineral phases is taken as evidence for precipitation at pressure–temperature conditions beyond antigorite stability.

The composition of infilling minerals in the fluid and their abundances have been estimated by means of scanning electron microscopy and microanalysis of opened inclusions, yielding approximately: 30 volume % magnetite ($Fe^{2+}_{0.78}Fe^{3+}_{1.98}Ti_{0.01}Cr_{0.09}Mn_{0.02}Mg_{0.2}Ni_{0.005}$); 25 volume % olivine ($Mg_{1.79}Fe_{0.18}Ti_{0.005}Cr_{0.001}Mn_{0.005}Si_1$); 25 volume % chlorite ($Mg_{5.05}Fe_{0.38}Ti_{0.01}Cr_{0.09}Mn_{0.004}Ni_{0.01}Al_{1.22}Si_{3.21}OH_8$); 20 volume % H_2O (to simplify the calculation apatite was not considered). From this information, the calculated mol fractions of major components in the fluid inclusions are as follows: $X_{Mg}=0.26$; $X_{Fe}=0.29$; $X_{Al}=0.02$; $X_{Si}=0.14$; $X_{OH}=0.3$; due to the high amount of magnetite the bulk inclusion compositions have $X_{Mg}=0.48$.

The trace element composition of the spinifex-like olivine (colorless and brown) and of its fluid+mineral inclusions was determined by means of LAM–ICP–MS microanalysis [29–33]. ICP–MS analyses were not performed on the early, pre-spinifex, aqueous saline inclusions hosted in serpentinites (Fig. 1A) due to their very small size (<10 μm). The spinifex-like olivine is essentially free of the measured trace elements, with the exception of Ti, Nb and Y in brown olivine (Table 2), which likely derive from fine-grained il-

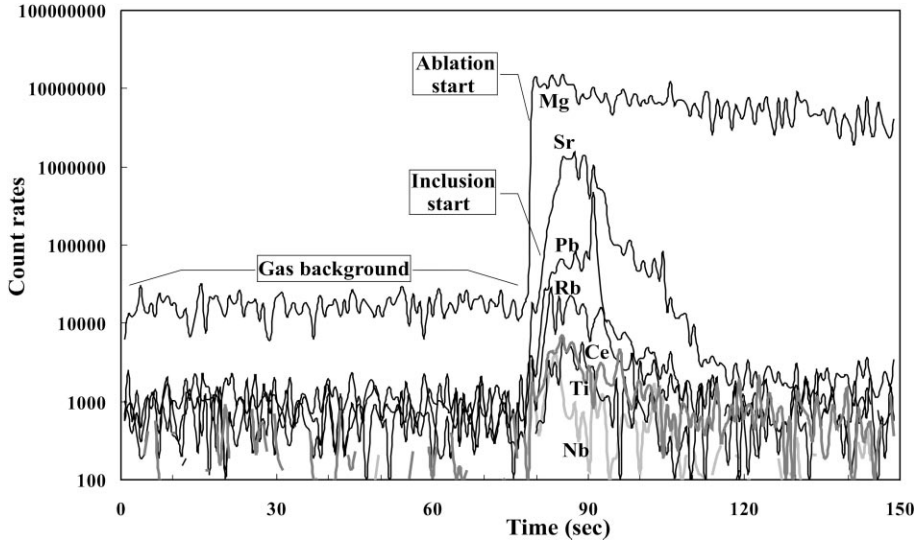

Fig. 3. Time-resolved analysis of fluid+mineral inclusions in the spinifex-like olivine. The analysis pertains to inclusion 5 of Table 1 and of Fig. 4B: it shows that Sr, Pb, Rb, Ce are within the background during ablation of olivine (at about 80 s) and rise up as soon as the laser beam reaches the fluid+mineral inclusion several μm below the olivine surface. The penetration of the laser beam into the inclusion is marked by the steep increase of the ion current of the elements not contained in olivine, and its exhaustion by the decrease of such signals to background level. The rise and fall are especially clear for Sr, always the most intense trace element signal. Thereafter, ablation continues into the host olivine. Different elements are likely hosted by different phases within the inclusion, so the evolution of their ion current with time depends on the position of each phase within the inclusion and on the way it undergoes ablation. The non-regular behavior (e.g. the spike in Pb) is not relevant to the analysis as the signals are integrated over the entire depth to obtain a bulk composition of the inclusion. Nb and Ti are also present in inclusion 5, but are absent in several other inclusion samples.

menite lamellae disseminated in this type of olivine. The time-resolved analysis of a representative fluid+mineral inclusion (inclusion 5; Table 2) is shown in Fig. 3: Sr, Pb, Rb and Ce are within background levels in olivine; their count rates rise significantly (up to 10^5 and 10^6 for Sr and Ba respectively) once the laser beam ablates the inclusion a few μm below olivine surface. All analyzed inclusions display high count rates for LILE and low counts for Ti, Nb and Y. Some inclusions in colorless olivine display higher Ti and Nb count rates than host olivine. Several inclusions in the brown olivine, disseminated with fine-grained ilmenite, have also shown Nb and Ti peaks: in this latter case, however, an estimate of the Nb and Ti content of the fluid+mineral inclusion was not attempted, since ablation may have affected the HFSE-rich ilmenite needles occurring in the surrounding brown olivine. Therefore, Table 2 and Fig. 4A do not include the HFSE values for the fluid+mineral inclusions hosted in brown olivine. Suitable mineral standards could not be used to quantify absolute trace element concentrations inside the inclusions, whereas trace element ratios are correct within statistics [33]. Table 2 and Fig. 4A report the Y-normalized ratios for a series of geochemically relevant trace elements.

The values of Table 2 were ratioed to the Y-normalized values of the primitive mantle (Fig. 4A) to allow comparison of the trace element signatures of the analyzed fluid+mineral inclusions with those of reference geological materials (available at the Geochemical Earth Reference Model GERM website, http://earthref.org/GERM), such as the composition of the continental crust, of global average subducted sediments, and of average MORB basalts. The trace element patterns of analyzed fluid+mineral inclusions display significant enrichment in many incompatible elements, with several LILE (such as Cs, Rb, Ba, Sr) and Pb showing higher concentrations compared to HFSE and rare earths. At a first glance, the overall pattern significantly differs (Fig. 4A) from those of typical MORB and shares the positive Ba, U, Pb, Sr and negative Nb spikes (although at much higher relative to Y absolute values) with recent volcanics from Mariana and Aleutian arcs

Table 2
Trace element compositions of spinifex-like olivines and relative to Y concentration ratios of fluid+mineral inclusions

	Al_2O_3 wt%	CaO wt%	Ba ppm	Rb ppm	Cs ppm	Th ppm	U ppm	Nb ppm	La ppm	Ce ppm	Pb ppm	Sr ppm	Nd ppm	Ti ppm	Y ppm
Spinifex olivine															
AL9854B	white olivine	< 0.01	< 0.06	< 1.1	< 0.4	< 0.2	b.d.l.	b.d.l.	0.05	< 0.05	< 0.02	< 0.4	< 0.5	< 0.15	21	< 0.08
AL9854B	white olivine	< 0.01	< 0.07	< 1.0	< 0.4	< 0.2	b.d.l.	b.d.l.	7.56	< 0.06	< 0.05	< 0.3	< 0.4	< 0.03	278	3.11
AL9854	brown olivine	< 0.01	< 0.18	< 1.7	< 3.4	< 1.4	b.d.l.	b.d.l.	0.43	< 0.11	< 0.05	b.d.l.	< 1.1	< 0.3	65	< 0.4
AL9854	brown olivine	< 0.01	< 0.19	< 2.1	< 4.3	< 1.7	b.d.l.	b.d.l.	< 0.70	< 0.15	< 0.11	b.d.l.	< 1.6	< 0.6	< 36	< 0.5
AL9564B	white olivine	< 0.01	< 0.08	< 1.3	< 1.7	< 0.6	b.d.l.	b.d.l.	1.44	< 0.16	< 0.12	b.d.l.	< 0.7	< 0.5	70	< 0.2
Fluid+mineral inclusions (relative to Y concentration ratios)																
AL9854B inc 1	white olivine			235	14.1	5.46		0.06		0.73	0.73	46.0	669	0.27	245	1.00
AL9854B inc 2	brown olivine			67.6	5.14	1.67		0.13		0.43	0.67	24.8	123	0.48		1.00
AL9854B inc 4	brown olivine			11.6	0.93	0.42	0.01	0.03		0.91	2.00	6.54	53.0	1.22		1.00
AL9854B inc 5	white olivine			149	7.77	3.34	0.03	0.25	0.90	0.73	1.20	43.7	426		105	1.00
AL9854B inc 8	white olivine			32.8	2.84	0.86		0.06		0.30	0.53	12.4	82.9	0.21		1.00
AL9854 inc 18	white olivine			60.0	4.00	1.36	0.05	0.14	3.68	0.45	0.86	16.3	176	0.43	1208	1.00

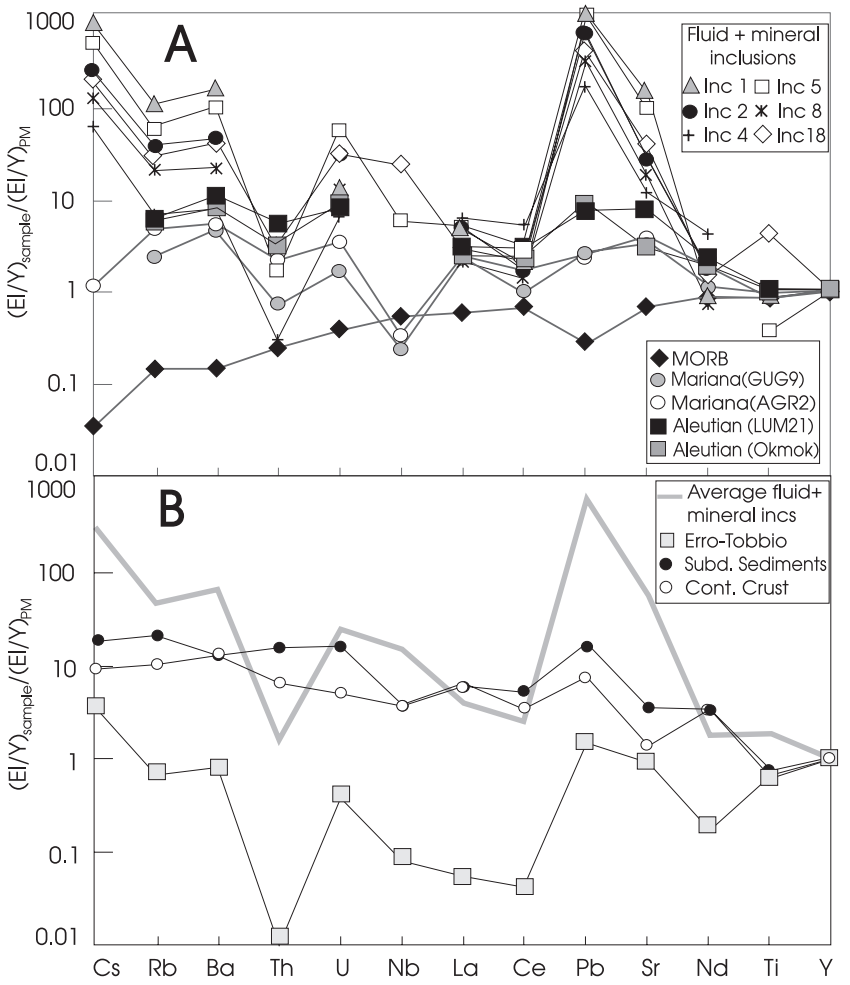

Fig. 4. Geochemical signatures of several representative fluid+mineral inclusions in spinifex-like olivine are compared to those of: (A) average MORB and representative lava samples from the Mariana arc (GERM, [35]); (B) continental crust, global subducted sediments and serpentinized peridotites from Erro-Tobbio (Western Alps, NW Italy) (GERM, [35,46]). The latter are regarded as possible precursors to a stage of antigorite breakdown; the complete dataset for Erro-Tobbio peridotites, including the elements not reported in [46], is deposited at the **Background Dataset**[1]. The element/Y ratios determined by LAM–ICP–MS are normalized to the corresponding element/Y values of the primitive mantle.

[20,35], which have geochemical features consistent with a dominant subducted sediment contribution. If the absolute values of relative to Y concentration ratios are considered, patterns of the analyzed fluid+mineral inclusions display closer similarities with those reported for both the continental crust and the global averaged subducted sediments (Fig. 4B), although discrepancies observed for LILE, Pb and Th are noticeable. Cs, Rb, Ba, Pb and Sr relative to Y are between one and two orders of magnitude higher, and that of Th relative to Y is one order of magnitude lower. In most inclusions Ba/Y, Rb/Y and Sr/Y values are about two orders of magnitude higher than Ti/Y and Nb/Y.

6. Discussion and conclusions

6.1. The fluid produced at antigorite breakdown

Two fluid populations were trapped by the Al-

mirez ultramafic rocks: (1) early H_2O-rich inclusions in serpentinites, dissolving up to 15 wt% chloride components and related to prograde subduction metamorphism in the antigorite stability field; (2) a later inclusion generation containing aqueous fluid+crystals in spinifex-like olivine derived from antigorite breakdown at peak pressure and temperature. Although early aqueous inclusions were involved in late-stage density readjustments, it appears that they do not record significant changes of the original fluid composition. Comparable fluids have been observed in other high to ultrahigh pressure terrains, where aqueous inclusions with variable salinities are diffusely found [6,7,11]. This early inclusion assemblage can thus be produced by continuous water loss during serpentinite burial as the result of dehydration reactions, producing metamorphic olivine plus fluid at the expense of serpentine and brucite [7].

The fluid inclusions primarily entrapped in the spinifex-like olivine are much different and have precipitated a number of solid phases plus a thin volume of aqueous liquid. Constancy of volume proportions of daughter phases inside this inclusion assemblage indicates trapping of a homogeneous (supercritical?) fluid loaded of dissolved components. The daughter mineral assemblage infilling such inclusions was likely precipitated in the stability field of olivine and chlorite, i.e. at high pressure and temperature conditions above the antigorite stability. However, our analysis indicates that average bulk major element compositions of these inclusions correspond to $X_{Mg} = 0.26$; $X_{Fe} = 0.29$; $X_{Al} = 0.02$; $X_{Si} = 0.14$; $X_{OH} = 0.3$. These concentrations are orders of magnitude higher than experimental solubilities measured at high pressure and temperature for the ultramafic system [36–38]. Experiments also indicate that in the pressure–temperature range of interest Al_2O_3 and SiO_2 have similar solubilities, which are much higher than those of MgO and FeO [37,38]. Therefore, the reconstructed bulk major element composition of the fluid+mineral inclusions and the high amounts of magnetite present in these inclusions cannot be explained by simple precipitation from the pristine antigorite dehydration fluid. Rather, loss of hydrogen and of major element components from the original fluid may be responsible for the observed magnetite abundance and for these extreme compositions. Experimental diffusion coefficients of hydrogen at 640–720°C, the crystallization temperature of the Almirez spinifex-like olivine, are very fast and correspond to 22×10^{-14} m^2 s^{-1} and 5×10^{-13} m^2 s^{-1} [39]; hydrogen loss from inclusions in olivine has moreover been documented by fluid inclusion studies [40,41]. This loss can be described by the model reaction $3Fe_2SiO_4$ (fayalite component)$+H_2O = 3SiO_{2(aq)} + Fe_3O_4+2H^+$. As a consequence of this reaction, magnetite is precipitated in the inclusion, and the X_{Mg} of olivine within the inclusion system increases. Olivine compositions support this process: the spinifex-like olivine away from the inclusions has a $X_{Mg} = 0.89$, whereas olivine precipitated in the inclusions has $X_{Mg} = 0.9$. Hydrogen loss from the fluid of the total system is also indicated by the fact that spinifex-like olivines contain a great number of microprecipitates of oxides [27]. At a larger scale, graphitic metapelites and metacarbonates surrounding the spinifex-like ultramafites could have acted as sinks for hydrogen. Olivine oxidation and hydrogen loss from the fluid are likely unrelated to retrograde post-entrapment modifications of fluid inclusions, and may have occurred before and/or during crystallization of the peak spinifex olivine+orthopyroxene assemblage. Constant volume proportions of magnetite and of silicate crystals in most inclusions (Fig. 1B,C) point to homogeneous hydrogen loss from all inclusions, a process unlikely to achieve during retrograde reequilibration of fluid inclusions. Lack of orthopyroxene inside the fluid+mineral inclusions is strong evidence that the above process was not a post-entrapment feature, but occurred at high pressure, before and/or during formation of the spinifex assemblage, as the result of complex fluid/rock interactions and olivine oxidation. The oxidation process thus may have developed during crystallization of the spinifex-like olivines and the $SiO_{2(aq)}$ produced may have contributed to formation of the coexisting

[1] http://www.elsevier.com/locate/epsl

spinifex enstatite. According to the above observations, solubility of major element components in the pristine dehydration fluid, probably with the exception of Al_2O_3 (1–2 wt%), cannot be approached because of the reactions between fluid and the surrounding olivine. An indication on the amount of silica originally dissolved in the aqueous fluid derives from the experimental work of Manning [37], showing that above 700°C and 1.5 GPa, aqueous fluids stable with olivine and orthopyroxene can dissolve 1–3 wt% SiO_2. Presence in the olivine-enstatite rocks of decimetric chlorite+orthopyroxene veins is a good field indication that an aluminum and silica-rich aqueous fluid was produced by the high pressure breakdown of antigorite. Differently from the fluid+mineral inclusions, reaction between fluid and fayalite end member and consequent hydrogen leakage did not affect the prograde liquid-rich aqueous inclusions in olivine ($X_{Mg} = 0.93$) of the serpentinites, because of their much lower iron content.

6.2. *Trace element composition of the antigorite breakdown fluid*

The fluid+mineral inclusions (Fig. 4A) are rich in incompatible elements. Their trace element patterns display progressively higher incompatible element abundances toward the left-hand side of Fig. 4A, with the exceptions of the prominent Pb and Sr positive anomalies and of the negative Th anomaly. This geochemical signature is surprising for a fluid phase produced from subducting hydrous mantle: compositions enriched in highly soluble elements are expected for fluid phases evolved from Earth reservoirs such as subducted crustal and sedimentary materials, whereas serpentinized mantle rocks are mainly viewed as major water carriers. Consequently, the fluid trapped in spinifex-like olivine either originated from (1) interaction between the fluid released at antigorite breakdown with fluids produced by external (crustal) rock sources, or from (2) dehydration of altered (serpentinized) oceanic mantle previously enriched in incompatible elements. Liberation of large amounts of fluid at antigorite breakdown induces rock fracturing [42] and enables fluid motion over appreciable length-scales, enhancing mixing of fluids from different rock sources to form a composite subduction fluid rich in incompatible elements. Average trace element analyses of MORB and crustal rocks (GERM website, http://earthref.org/GERM) are portrayed in Fig. 4B together with sediments from arc settings [35]. In terms of absolute incompatible element ratios, crustal and sedimentary rocks are the candidate reservoirs more closely approximating the compositions of the analyzed fluid+mineral inclusions. However, close inspection of the patterns shows that Cs, Th, Pb and Sr are highly discrepant. In particular, negative Th and huge positive Sr anomalies are not characteristic of sedimentary and continental materials [35]. Trace element patterns of the fluid+mineral inclusions therefore do not reflect sedimentary slab components, although they may indicate addition of fluid equilibrated with a high pressure paragenesis in metapelites [43]. Recent experiments indicate that fluids/melts equilibrated with phengite-bearing metasediments are enriched in LILE with respect to the solid residue [43]. Decoupling of Cs from Rb (Fig. 4A) may be due to preferential Rb retention in phengite within the pelite residue [44]. According to hypothesis (1), fractionation between La, Ce, and Ba, Rb can be controlled by presence of allanite in pelite [43], and the significant depletion in Th relative to U may be an effect of the oxidation process that occurred at inclusion entrapment. At oxidizing conditions U can become hexa-valent and can preferentially partition into aqueous fluids relative to Th [16], thus partly explaining the low Th/U ratios of the fluid+mineral inclusions. Lead is extremely abundant in the analyzed inclusions, in agreement with several works suggesting that Pb is more readily mobile in aqueous solutions than U and Th [19,45]. Marked Pb and Sr positive anomalies in the fluid, together with elevated Ba contents, could be partly inherited from pre-subduction enrichment of the serpentinite precursor. Hypothesis (1) therefore implies that analyzed fluid corresponds to a mixture of fluids equilibrated with different rock sources, and requiring a contribution from associated sedimentary slab components. Involvement of subducted sedimentary components in the genesis of metasomatic agents

for arc magmatism has been proposed by many authors ([35], with references).

An alternative scenario (hypothesis (2)) contemplates the internal elemental cycling during serpentine breakdown. Release of oceanic components into subduction fluids has been demonstrated by recent studies of high and ultrahigh pressure rocks, recording closed-system behavior and internal cycling of substances incorporated during shallow alteration [7,46,47]. Uptake of Sr, Ba, Cs Cl and alkalis can occur during alteration of oceanic mantle peridotites [46,48,49]. In the Almirez ultramafic rocks, bulk-rock Sr and Ba concentrations decrease from prograde antigorite serpentinites (Sr 7.6–21 ppm; Ba 72–280 ppm) to olivine-orthopyroxene spinifex-like rocks (Sr 3.9–7.6 ppm; Ba 38.7–0.97 ppm) [26]. Presence of these trace elements in fluid+mineral inclusions indicates that Ba and Sr were delivered to the fluid. Hydrothermal alteration may pre-concentrate Pb in the oceanic crust, thus increasing its potential for contribution to the subduction fluids [20,45]. Pre-subduction enrichment in Pb and Sr and their recycling in high pressure fluids may therefore originate the prominent positive Pb and Sr anomalies of Fig. 4A. Pb solubility in aqueous solutions is moreover enhanced by presence of dissolved chlorine [15]. Cl likely was an important component of fluid+mineral inclusions, as suggested by the presence of Cl-apatite daughter crystals (Fig. 1D), and by the occurrence of Cl-bearing inclusions in pre-spinifex serpentinites (Fig. 1A). Constraints to test the general validity of hypothesis (2) are limited, since very few trace element analyses of subducted serpentinites are presently available. Puga et al. [26] only report analyses of Ba and Sr, and the most complete dataset concerns the Erro-Tobbio high pressure serpentinite [46]. The latter records a subduction history analogous to the one of Cerro del Almirez serpentinites, and can reasonably be considered as precursor to a stage of antigorite breakdown [23,25,26]. Fig. 4B compares the average trace element patterns of the Erro-Tobbio serpentinites with the fluid+mineral Almirez inclusions, showing a close similarity between them. This is still more striking if one considers that serpentinites and fluids are from different localities, thus suggesting that their similarity is more than a mere coincidence. We therefore conclude that hypothesis (2) is the most likely: serpentinized oceanic mantle may produce the fluid compositions of Fig. 4 and may represent a valid candidate reservoir of elements and fluids for arc magmatism, as earlier proposed by Tatsumi et al. [14].

Considerably high lead concentrations in the analyzed fluid+mineral inclusions imply increase of the Th/Pb and U/Pb ratios in the residual slab, a feature recently taken to explain the trace element composition of mantle sources of several ocean island basalts [19]. Moreover, very low Ce/Pb ratios in the fluid+mineral inclusions are in good agreement with the experimental work of Brenan et al. [17], and with low Ce/Pb ratios of most arc lavas [20]. These features point that several LILE components in the fluid+mineral inclusions share relevant analogies with a typical fluid component of arc magmas (Fig. 4A). Main divergences are represented by the LILE/HFSE ratios. In the fluid+mineral inclusions portrayed in Fig. 4, Nb is one order of magnitude higher than Th, and is comparable to La and Ce. The arc lava compositions, together with all experimentally produced fluids, display huge depletions in Nb relative to Th, La, Ce and all other LILE components [12–19]. Th/Nb and La/Nb ratios < 1 thus indicate that HFSE are soluble in natural subduction fluids, as pointed out recently by several studies of fluid inclusions in high and very high pressure rocks [10,11]. Accordingly, the HFSE depletion characteristic of arc magmas should be ascribed to the selective HFSE extraction by HFSE-bearing phases (e.g. amphibole) during migration of slab-derived fluids through the mantle wedge [50,51].

Acknowledgements

This research has been supported by grants from the Italian MURST to the project 'Mineral reactions and chemical exchanges induced by fluid and melt migration through the Mantle' to G.B. Piccardo and R.V., from the Schweizerischer Nationalfonds No. 20-056867.99 to V.T. M.T.G.-P. and V.L.-S.V. acknowledge support by Project

BTE2000-1489 and Grupo RNM-0145 (Junta de Andalucía). Constructive reviews by O. Navon, C. Manning and T. Elliott have considerably improved the paper. We thank A. Stucky and E. Reusser for help during Raman spectroscopy, G.B. Piccardo, S. Poli, J. Connolly and P. Philippot for preliminary reviews and helpful comments. LAM–ICP–MS facilities at CNR-Centro di Studio per la Cristallochimica e la Cristallografia are gratefully acknowledged. *[BW]*

References

[1] Y. Tatsumi, Migration of fluid phases and genesis of basalt magmas in subduction zones, J. Geophys. Res. 94 (1989) 4697–4707.

[2] A.L. Boettcher, P.J. Wyllie, Phase relations in the system $NaAlSiO_4$–SiO_2–H_2O, Am. J. Sci. 267 (1969) 875–909.

[3] I.D. Ryabchikov, A.L. Boettcher, Experimental evidence at high pressure for potassic metasomatism in the mantle of the Earth, Am. Mineral. 65 (1980) 915–919.

[4] C.E. Manning, Effect of sediments on aqueous silica transport in subduction zones, in: G.E. Bebout, D.W. Scholl, S.H. Kirby, J.P. Platt (Eds.), Subduction: Top to Bottom, Geophysical Monograph, American Geophysical Union, 1996, pp. 277–284.

[5] K.H. Bureau, H. Keppler, Complete miscibility between silicate melts and hydrous fluids in the upper mantle: experimental evidence and geochemical implications, Earth Planet. Sci. Lett. 165 (1999) 187–196.

[6] P. Philippot, J. Selverstone, Trace element-rich brines in eclogitic veins: implications for fluid composition and transport during subduction, Contrib. Mineral. Petrol. 106 (1991) 417–430.

[7] M. Scambelluri, G.B. Piccardo, P. Philippot, A. Robbiano, L. Negretti, High salinity fluid inclusions formed from recycled seawater in deeply subducted alpine serpentinite, Earth Planet. Sci. Lett. 148 (1997) 485–500.

[8] T. Andersen, H. Austrheim, E.A.J. Burke, S. Elvevold, N_2 and CO_2 in deep crustal fluids: evidence from the Caledonides of Norway, Chem. Geol. 108 (1993) 113–132.

[9] O. Navon, I.D. Hutcheon, G.R. Rossman, G.J. Wasserburg, Mantle-derived fluids in diamond micro-inclusions, Nature 335 (1988) 784–789.

[10] P. Philippot, During subduction zone metamorphism, could the transition from aqueous solutions to silicate-rich hydrous fluids (or melts) be supercritical in nature?, J. Conf. Abstr. 1 (1996) 466.

[11] M. Scambelluri, P. Philippot, Deep fluids in subduction zones, Lithos 55 (2001) 213–227.

[12] M.T. McCulloch, J.A. Gamble, Geochemical and geodynamical constraints on subduction zone magmatism, Earth Planet. Sci. Lett. 102 (1991) 358–374.

[13] E. Stolper, S. Newman, The role of water in the petrogenesis of Mariana through magmas, Earth Planet. Sci. Lett. 121 (1994) 293–325.

[14] Y. Tatsumi, D.L. Hamilton, R.W. Nesbitt, Chemical characteristics of fluid phase released in from a subducted lithosphere and origin of arc magmas: Evidence from high-pressure experiments and natural rocks, J. Volcanol. Geotherm. Res. 29 (1986) 293–309.

[15] H. Keppler, Constraints from partitioning experiments on the composition of subduction-zone fluids, Nature 380 (1996) 237–240.

[16] J.M. Brenan, H.F. Shaw, F.J. Ryerson, D.L. Phinney, Mineral-aqueous fluid partitioning of trace elements at 900°C and 2.0 GPa: Constraints on the trace element chemistry of mantle and deep crustal fluids, Geochim. Cosmochim. Acta 59 (1995) 3331–3350.

[17] J.M. Brenan, H.F. Shaw, F.J. Ryerson, Experimental evidence for the origin of lead enrichment in convergent-margin magmas, Nature 378 (1995) 54–56.

[18] R. Stalder, S.F. Foley, G.P. Brey, I. Horn, Mineral-aqueous fluid partitioning of trace elements at 900–1200°C and 3.0–5.7 GPa: New experimental data for garnet, clinopyroxene, and rutile, and implications for mantle metasomatism, Geochim. Cosmochim. Acta 62 (1998) 1781–1801.

[19] T. Kogiso, Y. Tatsumi, S. Nakano, Trace element transport during dehydration processes in the subducted oceanic crust: 1. Experiments and implications for the origin of ocean island basalts, Earth Planet. Sci. Lett. 148 (1997) 193–205.

[20] D.M. Miller, S.L. Goldstein, C.H. Langmuir, Cerium/lead and lead isotope ratios in arc magmas and the enrichment of lead in the continents, Nature 368 (1994) 514–519.

[21] C.J. Hawkesworth, K. Gallagher, J.M. Hergt, F. McDermott, Trace element fractionation processes in the generation of island arc basalts, Phylos. Trans. R. Soc. A342 (1993) 179–191.

[22] P.B. Kelemen, K.T.M. Johnson, R.J. Kinzler, A.J. Irving, High-field strength-element depletion in arc basalts due to magma–mantle interaction, Nature 345 (1990) 521–524.

[23] M. Scambelluri, O. Muentener, J. Hermann, G.B. Piccardo, V. Trommsdorff, Subduction of water into the mantle: History of an alpine peridotite, Geology 23 (1995) 459–462.

[24] P. Ulmer, V. Trommsdorff, Serpentine stability to mantle depths and subduction-related magmatism, Science 268 (1995) 858–861.

[25] V. Trommsdorff, V. Lòpez-Sànchez Vizcaino, M.T. Gòmez-Pugnaire, O. Muentener, High pressure breakdown of antigorite to spinifex-textured olivine and orthopyroxene, SE Spain, Contrib. Mineral. Petrol. 132 (1998) 139–148.

[26] E. Puga, J.M. Nieto, A. Dìaz de Federico, J.L. Bodinier, L. Morten, Petrology and metamorphic evolution of ultramafic rocks and dolerite dykes of the Betic Ophiolitic Association (Mulhacén Complex, SE Spain): Evidence of eo-Alpine subduction following and ocean-floor metasomatic process, Lithos 49 (1999) 23–56.

[27] M.D. Ruiz Cruz, E. Puga, J.M. Nieto, Silicate and oxide exsolution in pseudo-spinifex olivine from metaultramafic rocks of the Betic Ophiolitic Association: A TEM study, Am. Mineral. 84 (1999) 1915–1924.
[28] M.T. Gòmez-Pugnaire, G. Franz, V. Lòpez-Sànchez Vizcaino, Retrograde formation of NaCl-scapolite in high pressure metaevaporites from the Cordilleras Béticas (Spain), Contrib. Mineral. Petrol. 116 (1994) 448–461.
[29] R.P. Taylor, S.E. Jackson, H.P. Longheric, J.D. Webster, In situ trace-element analysis of individual silicate melt inclusions by laser ablation microprobe–inductively coupled plasma–mass spectrometry (LAM–ICP–MS), Geochim. Cosmochim. Acta 61 (1997) 2559–2567.
[30] P. Bottazzi, M. Tiepolo, R. Vannucci, A. Zanetti, R.C. Brumm, S.F. Foley, R. Oberti, Distinct local configurations for heavy and light REE in amphibole and the prediction of $^{Amph/L}D_{REE}$, Contrib. Mineral. Petrol. 137 (1999) 36–45.
[31] H.P. Longerich, S.E. Jackson, D. Gunther, Laser ablation inductively coupled plasma mass spectrometric transient signal data acquisition and analyte concentration calculation, J. Anal. At. Spectrom. 11 (1996) 899–904.
[32] D. Günther, Quantitative fluid inclusion analysis using a 193 nm excimer laser-ablation system coupled to ICP–MS, in: P. Sylvester (Ed.), Laser-Ablation-ICPMS in the Earth Sciences, Principles and Applications, Mineralogic Association of Canada, Short Course Series 29, 2001, pp. 47–61.
[33] B.J. Fryer, S.E. Jackson, H.P. Longerich, The design, operation and role of the laser-ablation microprobe coupled with an inductively coupled plasma-mass spectrometer (LAM–ICP–MS) in the earth sciences, Can. Mineral. 33 (1995) 303–312.
[34] R.W. Potter, M.A. Clynne, D.L. Brown, Freezing point depression of aqueous sodium chloride solutions, Econ. Geol. 73 (1978) 284–285.
[35] T. Elliott, T. Plank, A. Zindler, W. White, B. Bourdon, Element transport from slab to volcanic front in the Mariana arc, J. Geophys. Res. 102 (1997) 14991–15019.
[36] M.E. Schneider, D.H. Eggler, Fluids in equilibrium with peridotite minerals: Implications for mantle metasomatism, Geochim. Cosmochim. Acta 50 (1986) 711–724.
[37] C.E. Manning, Phase-equilibrium controls on SiO_2 metasomatism by aqueous fluid in subduction zones: Reaction at constant pressure and temperature, Int. Geol. Rev. 37 (1995) 1074–1093.
[38] Y.G. Zhang, J.D. Frantz, Enstatite–forsterite–water equilibria at high temperatures and pressures, Am. Mineral. 85 (2000) 918–925.
[39] S.J. Macwell, D.L. Kohlstedt, Diffusion of hydrogen in olivine: Implications for water in the mantle, J. Geophys. Res. 95 (1990) 5079–5088.
[40] D.L. Hall, S.M. Sterner, Experimental diffusion of hydrogen into synthetic fluid inclusions in quartz, J. Metamorf. Geol. 13 (1995) 345–355.
[41] J.A. Mavrogenes, R.J. Bodnar, Hydrogen movement into and out of fluid inclusions in quartz: Experimental evidence and geologic implications, Geochim. Cosmochim. Acta 58 (1994) 141–148.
[42] L.A. Reinen, H.W. Green, S.K. Nielsen, Dehydration embrittlement of antigorite serpentinite at high-pressures: implications for intermediate depth earthquakes, Proceedings AGU Fall Meeting, supplement to EOS, AGU 79, 1998, p. 853.
[43] J. Hermann, D.H. Green, Experimental constraints on high pressure melting in subducted crust, Earth Planet. Sci. Lett. 188 (2001) 149–168.
[44] S. Melzer, B. Wunder, Island arc basalt alkali ratios: Constraints from phengite-fluid partitioning experiments, Geology 28 (2000) 583–586.
[45] A.W. Hofmann, Mantle geochemistry: The message from oceanic volcanism, Nature 385 (1997) 219–228.
[46] M. Scambelluri, E. Rampone, G.B. Piccardo, Fluid and element cycling in subducted serpentinite: A trace element study of the Erro-Tobbio high-pressure ultramafites (Western Alps, NW Italy), J. Petrol. 42 (2001) 55–67.
[47] P. Philippot, P. Agrinier, M. Scambelluri, Chlorine cycling in the subducted oceanic lithosphere, Earth Planet. Sci. Lett. 161 (1998) 33–44.
[48] E. Bonatti, J. Honnorez, G. Ferrara, Equatorial Mid-Atlantic Ridge: petrologic and Sr isotopic evidence for alpine-type rock assemblage, Earth Planet. Sci. Lett. 9 (1970) 247–256.
[49] M.A. Menzies, A. Long, G. Ingram, M. Tatnel, D. Janecky, MORB–peridotite–sea water interaction: experimental constraints on the behaviour of trace elements, $^{87}Sr/^{86}Sr$ and $^{143}Nd/^{144}Nd$ ratios, in: H.M. Prichard, T. Alabaster, N.B.W. Harris, C.R. Neary (Eds.), Magmatic Processes and Plate Tectonics, Geological Society Special Publication 76, 1993, pp. 309–322.
[50] D.A. Ionov, A.W. Hofmann, Nb–Ta-rich mantle amphiboles and micas: Implications for subduction-related metasomatic trace element fractionations, Earth Planet. Sci. Lett. 131 (1995) 341–356.
[51] M. Tiepolo, R. Vannucci, R. Oberti, S. Foley, P. Bottazzi, A. Zanetti, Nb and Ta incorporation and fractionation in titanian pargasite and kearsutite: crystal-chemical constraints and implications for natural systems, Earth Planet. Sci. Lett. 176 (2000) 185–201.